International Journal of Refrigeration 183 (2026) 188–198

Contents lists available at ScienceDirect

International Journal of Refrigeration

journal homepage: www.elsevier.com/locate/ijrefrig

INSTITUT INTERNATIONAL DU FROID
INTERNATIONAL INSTITUTE OF REFRIGERATION

Experimental measurements and molecular simulations for *pvTz* properties of carbon dioxide (CO_2) + 1,1-difluoroethylene (R1132a) binary system in the two-phase and superheated vapor regions

Sebastiano Tomassetti [a,*], Lorenzo Merlonghi [b], Tomoaki Imai [c], Giovanni Di Nicola [a,d], Chieko Kondou [c]

[a] *Dipartimento di Ingegneria Industriale e Scienze Matematiche, Università Politecnica delle Marche, via Brecce Bianche 12, 60131 Ancona, Italy*
[b] *Department of Civil, Chemical, Environmental and Material Engineering, (DICAM), Alma Mater Studiorum – Università di Bologna, Via Terracini 28, 40131, Bologna, Italy*
[c] *Graduate School of Engineering, Nagasaki University, 1-14, Bunkyo, 852-8521 Nagasaki, Japan*
[d] *ITC-CNR, Construction Technologies Institute, National Research Council, Padova, Italy*

ARTICLE INFO

Keywords:
Carbon dioxide (R-744)
1,1-difluoroethylene (HFO-1132a)
Molecular simulation
VLE assessment
ULT refrigeration

ABSTRACT

This study provides 23 two-phase and 133 vapor-phase pressure-specific volume-temperature-composition (*pvTz*) measurements for the mixture containing carbon dioxide (CO_2) and 1,1-difluoroethylene (R1132a), considered a potentially low global warming potential (GWP) alternative for ultralow temperature refrigeration systems. Vapor-liquid equilibrium (VLE) and vapor-phase *pvTz* properties predicted through molecular dynamics (MD) simulations are also presented. An isochoric apparatus was used to measure the properties for ten CO_2 mole fractions along ten isochores with specific volumes equal to (0.016846, 0.018521, 0.028775, 0.029922, 0.029931, 0.032358, 0.037241, 0.039089, 0.052176, 0.083492) $m^3\ kg^{-1}$ in the temperature and pressure ranges from (228.15 to 303.15) K and from (404.5 to 2519.9) kPa, respectively. The two-phase measurements were used to assess the VLE of the binary system by the flash method with the Peng-Robinson (PR) and PC-SAFT equations of state (EoSs), yielding average absolute relative deviations (AARDs) between experimental and calculated pressures of 0.20% and 0.19%, respectively. The values calculated with the PR and PC-SAFT EoSs showed qualitative agreement with the VLE properties from MD simulations, yielding AARD(*p*) of 3.44 % and 3.32 %, respectively. The measurements carried out in the superheated vapor region were compared with calculations from the PR and PC-SAFT EoSs, obtaining low deviations (AARD(*p*) of 0.38 % for the PR EoS and 0.33 % for the PC-SAFT EoS). Finally, a qualitatively good agreement between the MD simulations and the EoS calculations was also observed in the superheated vapor region (AARD(*p*) of 1.02 % for the PR EoS and 1.00 % for the PC-SAFT EoS).

1. Introduction

Currently, the refrigeration industry has the need to identify low global warming potential (GWP) refrigerants as suitable alternatives to the working fluids commonly used in ultralow temperature (ULT) refrigeration systems, which allow the products' preservation at temperatures lower than -50°C. Although this application was not directly considered in the environmental regulations to limit the GWP of refrigerants used in refrigeration, air conditioning, and heat pump (RACHP) systems (Mota-Babiloni et al., 2020), the availability of the mainly used refrigerants for ULT systems, i.e., R23 and R508B, could be negatively affected by international regulations and agreements due to their very high GWP. Soon, these refrigerants could become unavailable or too expensive because of the reduction in the production and use of high GWP refrigerants established by the Kigali Amendment to the Montreal Protocol (Polonara et al., 2017; UNEP, 2016) and the limited quotas for placing them on the market imposed by international regulations (METI, 2019; Regulation (EU) No. 2024/573, 2024).

Various natural and synthetic fluids with low GWP, known as 4th generation refrigerants (Domanski and McLinden, 2025; McLinden and Huber, 2020), are currently being studied as potential alternatives for several RACHP applications, particularly in form of mixtures (Giménez-Prades et al., 2025; Hao et al., 2025, 2024). Some 4th

* Corresponding author.
E-mail address: s.tomassetti@univpm.it (S. Tomassetti).

https://doi.org/10.1016/j.ijrefrig.2026.01.002
Received 28 August 2025; Received in revised form 4 December 2025; Accepted 1 January 2026
Available online 5 January 2026
0140-7007/© 2026 The Author(s). Published by Elsevier B.V. This is an open access article under the CC BY license (http://creativecommons.org/licenses/by/4.0/).

Nomenclature

Latin symbols

c	Speed of sound (m s^{-1})
c_v^0	Ideal gas specific heat capacity at constant volume (kJ•kg^{-1}•K^{-1});
k_{12}	Binary interaction parameter;
m	Sample mass (g) and segment length;
M	Molar mass (g mol^{-1})
n	Number of moles charged (mol);
N	Number of experimental data;
p	Pressure (kPa);
q	Partial charge (C);
Q	Objective function of the "flash method";
r_{ij}	Distance between two non-bonded atoms i and j (m);
T	Temperature (K);
U	Expanded uncertainty;
$U_{non\text{-}bonded}$	Nonbonding energy (J mol^{-1});
v	Specific volume (m^3•kg^{-1});
x_i	Liquid phase mole fraction of i-th component;
y_i	Vapor phase mole fraction of i-th component;
z_i	Bulk mole fraction of i-th component;

Greek symbols

ε/k	Segment energy (K);
ε_0	Vacuum permittivity (F m^{-1});
ε_{ij}	Lennard–Jones potential energy (J mol^{-1});
ρ	Density (kg m^{-3});
σ	Segment diameter (Å);
σ_{ij}	Lenard-Jones potential collision diameter (m);
ω	Acentric factor;

Acronyms

AARD	Absolute average relative deviation;
EoS	Equation of state;
GC	Gas chromatography;
GWP	Global warming potential;
HFC	Hydrofluorocarbon;
HFO	Hydrofluoroolefines;
MD	Molecular dynamics;
PC-SAFT	Perturbed-chain statistical associating fluid theory;
PR	Peng-Robinson;
RACHP	Refrigeration, air conditioning, and heat pump;
ULT	Ultralow temperature;
VLE	Vapor-liquid equilibrium;

Subscripts/Superscripts

b	Normal boiling point;
c	Critical;
calc	Calculated;
exp	Experimental;
l	Liquid;
sat	Saturated;
sim	Simulated;
t	Triple point;

generation refrigerants are considered promising alternatives for the ULT applications, such as ethane (R170), ethylene (R1150), carbon dioxide (R744), fluoromethane (R41) and 1,1-difluoroethene (R1132a) (Mota-Babiloni et al., 2020). In this regard, low GWP mixtures containing some of these refrigerants have been studied as suitable working fluids for the low-temperature stage of ULT two-stage cascade refrigeration systems, Linde-Hampson refrigeration systems, or Joule-Thomson refrigeration systems (Mota-Babiloni et al., 2023). Various works evaluating mixtures containing natural refrigerants, especially carbon dioxide (CO_2), have been proposed in the scientific literature (Bai et al., 2021; Di Nicola et al., 2011; Massuchetto et al., 2019; Mota-Babiloni et al., 2023; Sobieraj and Rosiński, 2019). The increasing interest in mixtures based on CO_2 for ULT applications is further evidenced by R469A (35 mass% CO_2/32.5 mass% R32/32.5 mass% R125) with GWP = 1357, R472A (69 mass% CO_2/19 mass% R134a/12 mass% R32) with GWP = 353, and R473A (60 mass% CO_2/20 mass% R1132a/10 mass% R23/10 mass% R125) with GWP = 1830, which were recently proposed as lower GWP alternatives for these applications (Mota-Babiloni et al., 2023). In fact, the three mixtures registered in the ASHRAE Standard 34-2022 (ASHRAE Standard, 2022) contain CO_2 and other synthetic refrigerants, such as hydrofluorocarbons (HFCs) and hydrofluoroolefins (HFOs).

On the other hand, ULT refrigeration systems working with mixtures containing R1132a have been analyzed in a limited number of studies (Mota-Babiloni et al., 2023; Qin et al., 2023, 2021a, 2021b). This aspect could be because, although this ethylene derivative HFO is considered a promising low GWP mixture component for ULT systems (Mota-Babiloni et al., 2016), models to accurately describe the thermophysical properties of R1132a and its mixtures are not yet available in the scientific literature. While the measurements of different thermophysical properties for this HFO were recently published in the literature, such as critical point properties (Low, 2018; Perera et al., 2023), triple point temperature (Tomassetti et al., 2022a), saturation properties (Low, 2018; Perera et al., 2023; Thu et al., 2023; Tomassetti and Di Nicola, 2021), vapor and liquid pvT properties (Perera et al., 2023; Tomassetti and Di Nicola, 2021), speed of sound (Demirdesen et al., 2023; Rowane and Perkins, 2024), only a preliminary Helmholtz energy equation of state (EoS) in the Span-Wagner format was developed by Low (2018). However, this EoS is not available in commercial software (Bell, 2025), such as REFPROP 10.0 (Lemmon et al., 2018).

As for mixtures containing R1132a, a very limited number of measurements for their thermophysical properties are currently available in the literature (Bell et al., 2021). In particular, only two works reporting experimentally determined thermodynamic properties for the binary mixture containing CO_2 and R1132a have been found. The solid-liquid equilibrium (SLE) of CO_2 + R1132a binary system was measured through two experimental setups based on the cooling curve method by Tomassetti et al. (2022b). Their results showed that the mixture had an eutectic behavior well described by the Schröder equation.

Recently, Menegazzo et al. (2025) measured the compressed-liquid and vapor densities for two compositions of CO_2 + R1132a binary system through a two-sinker densimeter. The measurements were carried out in the temperature range from 220 K to 350 K with pressures up to 30 MPa. Moreover, the measurements of the compressed-liquid speed of sound for the same two compositions were carried out using a pulse-echo-type instrument for temperatures between 230 K and 350 K and pressures up to 65 MPa. Finally, a mixture model based on the multi-fluid Helmholtz-energy explicit model was developed for the CO_2+R1132a binary system on the basis of the experimental data. The Helmholtz energy EoS for CO_2 proposed by Span and Wagner (1996) and the preliminary EoS for R1132a proposed by Low (2018) were used in the presented model. A good agreement between the experimental data and the model calculations was found.

To compensate for the lack of an adequate number of measurements for the thermophysical properties of 4th generation refrigerants and their mixtures, molecular dynamics (MD) simulation has been employed to provide reliable predictions that can be complementary to the experimental data (Raabe, 2019, 2016). Studies reporting MD simulations on

the vapor-liquid equilibrium of various mixtures containing potential low GWP refrigerants, i.e., 2,3,3,3-tetrafluoro-1-propene (R1234yf), *trans*-1,3,3,3-tetrafluoro-1-propene (R1234ze(E)), *cis*-1,1,1,4,4,4-hexafluoro-2-butene (R1336mzz(Z)), *trans*-1-chloro-3,3,3-trifluor-opropene (R1233zd(E)), and trifluoroethylene (R1123), have been proposed by Raabe (2019, 2015, 2013). Some of these predictions were used for the development of specific EoSs for the mixtures (Raabe, 2016). Recently, the vapor-liquid equilibrium of CO_2 + R1132a binary system was simulated through MD simulation by the author's group (Imai et al., 2023). Moreover, MD simulation results for the transport properties of different alternative refrigerants have been reported in various literature studies, such as the viscosity of R1234yf, R1234ze(E), R1233zd(E), *cis*-1-chloro-2,3,3,3-tetrafluoropropene (R1224yd(Z)), and R1336mzz (Z) (Fouad and Alasiri, 2020) and the surface tension of the following binary mixtures: R1234yf + propane (R290) and R1234yf + isobutane (R600a) (Fouad and Vega, 2018), and R1123 + trifluoro-iodomethane (CF_3I) (Kawahara et al., 2023).

In this study, 23 vapor-phase and 133 two-phase pressure-specific volume-temperature-composition (*pvTz*) properties for the CO_2 + R1132a binary system measured with an isochoric apparatus are presented. The VLE properties of the binary system under study were derived from the two-phase measurements using a theoretical approach based on the "flash method" with different EoSs. A comparison between the vapor-phase experimental points and the calculations provided by different models is also reported. The experimental measurements and EoS predictions were further compared with MD simulations. Although the MD simulations are less accurate than the experimental data, they provide results over a wider range of conditions and were therefore employed to assess the reliability of the EoS predictions beyond the experimental range. The proposed EoSs were compared with MD simulations for VLE properties and superheated vapor *pvTz* data at temperatures of 300–400 K to verify the validity of the EoSs in the extrapolated region.

2. Materials and methods

This section provides details regarding the measured samples, the experimental apparatus, and the measurement procedure. The calculation methods used to correlate the proposed measurements are also described.

2.1. Materials

Table 1 presents sample information of carbon dioxide (R744, CO_2, CAS number 124-38-9) and 1,1-difluoroethene (R1132a, $C_2H_2F_2$, CAS No. 75-38-7), together with their molar mass, critical properties, acentric factor, normal boiling point temperature, and triple point temperature. The purity of the samples was analyzed through a gas chromatograph (GC) with a thermal conductivity detector. The non-condensable gases of the CO_2 sample were removed by subjecting it to several cycles of freezing, evacuation, thawing, and ultrasonic stirring.

2.2. Apparatus and measurement procedure

The isochoric apparatus was widely described in previous studies (Brown et al., 2017; Di Nicola et al., 2005; Giuliani et al., 1995) together with the experimental procedure and uncertainties. Consequently, only the key features are summarized below. The experimental setup, shown in Fig. 1, allows to measure the *pvTz* properties from (210 to 380) K by employing two thermostatic baths. The target temperature is set using a PID device connected to a 25-ohm platinum resistance thermometer (Hart Scientific 5680). The measurement cell is an AISI 304 stainless steel sphere with a volume of approximately 273.5 cm^3 at 298 K. This sphere is connected to a differential Ruska 7000 pressure transducer combined with an electronic null indicator.

The samples were charged in the experimental setup by a gravimetric method involving the following steps:

1. After weighing a container charged with the lower-pressure refrigerant and an evacuated container through a Sartorius MC 1

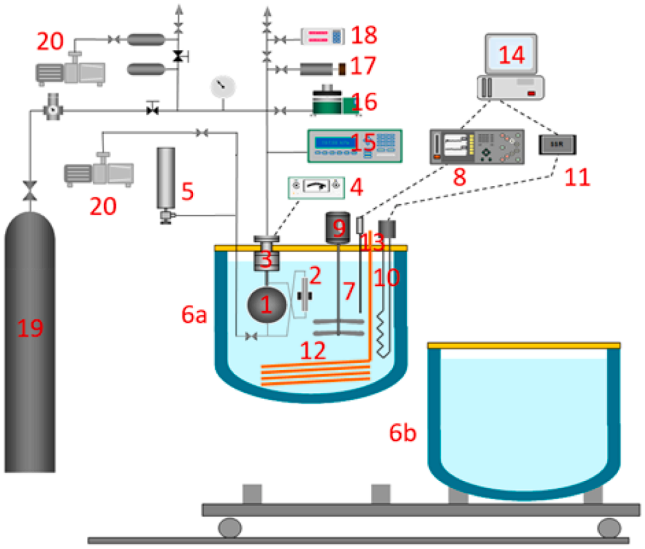


Fig. 1. Isochoric apparatus scheme.

Table 1
Sample information, molar mass (M), critical temperature (T_c), critical pressure (p_c), acentric factor (ω), normal boiling point temperature (T_b), and triple point temperature (T_t) of CO_2 and R1132a.

Chemical Name	M/g mol^{-1}	T_c/K	p_c/kPa	ω	T_b/K	T_t/K	Source	Initial Mole Fraction Purity	Purification Method	Final Mole Fraction Purity	Analysis Method
CO_2[a]	44.009	304.13[b]	7377.3[b]	0.22394[b]	194.69[b]	216.50[c]	Sol SpA	99.99%	several cycles of freezing, evacuation, melting, and ultrasonic agitation	99.99%	GC
R1132a[d]	64.035	302.62[e]	4448.0[e]	0.17600[e]	189.08[f]	111.00[c]	Mexichem UK Limited	99.9%	None	-	GC

[a] Carbon dioxide
[b] Reported by Lemmon et al. (2018)
[c] Reported by Tomassetti et al. (2022a)
[d] 1,1-difluoroethene
[e] Reported by Perera et al. (2023)
[f] Reported by Thu et al. (2023)

electronic balance (uncertainty of 0.025 g), these containers were connected to the apparatus with a vacuum pump.
2. The vacuum pump was employed to evacuate the isochoric sphere, tubing, and connections.
3. A specific mass of refrigerant was loaded into the measuring cell.
4. The vacuumed container was used to recover the refrigerant remaining in the connection tubing.
5. After disconnecting the charging and recovering containers from the apparatus, they were weighed again.
6. The discharged and recovered sample amounts were determined as the difference between the initial and final masses of the containers. Consequently, the difference between these two masses allowed us to calculate the amount of the first refrigerant charged in the isochoric sphere.
7. The same procedure was followed to load the higher-pressure refrigerant.

As explained in previous works (Giuliani et al., 1995; Di Nicola et al., 2005), the expanded uncertainty at the 95 % confidence level (coverage factor of 2) for the temperature was determined from the propagation of uncertainty by considering the accuracy of the thermometer and the bath instability, obtaining a value equal to 0.03 K. The expanded uncertainty for the pressure measurements was found to be 1 kPa by taking into account the uncertainty of the transducer, null indicator system, the pressure gauges, and the temperature fluctuations due to bath instability. The expanded uncertainty for the volumes was estimated to be 0.3 cm^3 from the calibration procedure used to determine the volume of the measuring cell. The procedure based on the propagation of uncertainty reported by Tomassetti et al. (2020b) was employed to determine the expanded uncertainty of the mass, that is equal to 0.1 g. As described elsewhere (Brown et al., 2018, 2017), the uncertainty of the specific volumes was calculated by considering the uncertainties of the volume estimation and mass measurements It ranges between (0.000209 and 0.005107) $m^3 \bullet kg^{-1}$. The uncertainty for the mole fractions was derived from the uncertainties of the mass measurements, obtaining values from 0.0040 to 0.0213.

The measurement procedure consisted of the following steps:

1. The temperature of the thermostatic bath was set equal to the target temperature and allowed to stabilize.
2. A circulating pump was turned on for a few minutes.
3. The sample charged in the apparatus was allowed to stabilize for an hour.
4. The pressure values were measured.
5. The next measurement was carried out by repeating the previous steps.

2.3. Molecular dynamics simulation

The thermal equilibrium properties of the CO_2+R1132a binary system were calculated using GROMACS 2016 (Abraham et al., 2015). Table 2 summarizes the methods and simulation parameters used in the MD calculations. OPLS-AA/L type formula (Jorgensen et al., 1996) was employed to compute potential energies. The formula includes harmonic bond-stretching and angle-bending terms, as well as periodic proper dihedral potentials for bonded interactions. Non-bonded interactions were modeled using Coulombic and van der Waals forces, the latter described by the 12-6 Lennard–Jones potential.

$$U_{\text{non-bonded}} = \sum \frac{q_i q_j}{4\pi\varepsilon_0 r_{ij}} + \sum 4\varepsilon_{ij}\left[\left(\frac{\sigma_{ij}}{r_{ij}}\right)^{12} - \left(\frac{\sigma_{ij}}{r_{ij}}\right)^{6}\right] \quad (1)$$

where $U_{\text{non-bonded}}$ is the nonbonding energy, q_i and q_j are the partial charge of atoms i and j, ε_0 is the vacuum permittivity, r_{ij} is the distance between two non-bonded atoms i and j, σ_{ij} is the Lenard-Jones potential collision diameter, and ε_{ij} is the Lenard-Jones potential energy.

Table 2
Methods and options employed in MD simulations.

Parameter	Method/option
Code	GROMACS 2016 double precision[a]
Number of molecules	2000 ~ 5000
Boundary	Periodic for all sides of a simulation cell box
Integrator	Leap-flog [b, c]
Ensemble	NVT
Velocity generation	Maxwell distribution with random seed with NVT ensemble
Time step	0.5 fs
Equilibration period	4 – 10 ns
Sampling period	2 – 3 ns
van der Waals cutoff	1.5 nm
Coulomb	Particle-mesh Ewald [d]
Coulomb cutoff	1.5 nm
Temperature coupling	Nose-Hoover chain [e, f]
Holonomic constraints	Hydrogen bonding (w/o angle constraint) using LINCS algorithm [g]

[a] Abraham et al. (2015).
[b] Berendsen et al. (1995).
[c] Cuendet and Van Gunsteren (2007).
[d] Darden et al. (1993).
[e] Nosé (1984).
[f] Hoover (1985).
[g] Hess et al. (1997).

Interactions between atoms separated by three covalent bonds (i.e., 1–4 interactions) were scaled by a factor of 0.5. The Lennard–Jones parameters σ_{ij} and ε_{ij} were determined using the Lorentz–Berthelot combining rules for heteroatomic combinations, despite their known limitations (Delhommelle and Millié, 2001). The force field parameters for R1132a and CO_2 were adjusted based on the general OPLS-AA/L model (Jorgensen et al., 1996) and the EPS2 model (Harris and Yung, 1995), respectively, to reproduce the experimental saturation densities. Detailed information on the force field parameters used in this study are provided in the Supplementary Information (SI_1). Those numbers are listed in the form of a topology file available in GROMACS.

The pressure was averaged over 2–3 ns after equilibration. In the case of superheated vapor calculations, the averages in three directions (x, y, and z directions) were taken because of the isotopy assumption. In the case of vapor-liquid equilibrium calculations, the pressure tensor perpendicular to the liquid film was averaged over the simulation box cell.

2.4. Data correlation

The two-phase isochoric measurements were used to derive the vapor-liquid equilibrium (VLE) properties for CO_2 + R1132a binary system (i.e., p, liquid (x_i) and vapor (y_i) mole fractions) through a procedure based on the "flash method" presented in previous studies (Di Nicola et al., 1998; Tomassetti et al., 2020a). The following equations of state (EoSs) were employed in the procedure: the Peng Robinson (PR) EoS (Peng and Robinson, 1976) with the standard one-binary-parameter mixing rules and the perturbed-chain statistical associating fluid theory (PC-SAFT) EoS (Gross and Sadowski, 2001) coupled with the conventional Berthelot-Lorentz mixing rules. The well-known PR EoS was selected since it is widely used in the refrigeration industry because of its simplicity and ease of application to new refrigerants, such as R1132a (Bell et al., 2019). In addition, the accuracy of the more complex PC-SAFT EoS was also evaluated for calculating the thermodynamic properties of the studied mixture, since its generally good capability in describing the VLE and $pvTx$ properties of binary systems containing HFOs (Peng et al., 2024).

The binary interaction parameter (k_{12}) of the mixing rules considered for the VLE assessment was derived through the following objective function (Q):

$$Q = \sum_{i=1}^{N} \left(\frac{p_{\mathrm{exp},i} - p_{\mathrm{calc},i}}{p_{\mathrm{exp},i}} \right)^2 \quad (2)$$

where N is the number of experimental data.

The PR EoS and the PC-SAFT EoS were also used to correlate the *pvTz* properties measured in the superheated vapor region by using k_{12} determined through the procedure based on the "flash method".

The open-source library teqp (Bell et al., 2022) was adopted to implement the models. The critical properties and acentric factors of the pure fluids reported in Table 1 were considered for the calculations. The following PC-SAFT parameters for CO_2 provided by Anoune et al. (2021) were employed in this study: segment length (m) of 2.66827, segment diameter (σ) of 2.61212 Å, and segment energy (ε/k_b), i.e., the depth pair potential divided by the Boltzmann constant (k_b), of 147.234 K. These parameters were determined from the fitting of vapor pressure and liquid density measurements, ensuring also accurate critical point calculations of non-associating compounds, which are essential for the description of the VLE of mixtures at high temperatures and pressures.

On the other hand, the only available PC-SAFT parameters for R1132a were estimated by Outcalt and Rowane (2022) using the correlations proposed by Anoune et al. (2021) with the critical properties and acentric factor measured by Low (2018), i.e., $T_c = 302.81$ K, $p_c = 4461.0$ kPa, and $\omega = 0.18100$. These parameters correspond to the values labelled as Set A in Table 3. However, it is worth noting that these estimated parameters change if different critical properties and acentric factor are used in the correlations of Anoune et al. (2021). For example, using the physical properties reported in Table 1, new PC-SAFT parameters for R1132a can be derived. They are reported in Table 3 as Set B.

Considering the different sets of PC-SAFT parameters available for R1132a, it is worth evaluating their accuracy in the calculation of the properties of the pure fluid. Table 4 presents the deviations between the calculated values and the experimental saturated pressures (p_{sat}), saturated liquid and vapor densities ($\rho^{\mathrm{l}}_{\mathrm{sat}}$ and $\rho^{\mathrm{v}}_{\mathrm{sat}}$), density in the subcooled liquid (ρ^{l}), pressures in the superheated vapor regions (p^{v}), and speed of sound (c), collected from the literature (Demirdesen et al., 2023; Perera et al., 2023; Rowane and Perkins, 2024; Thu et al., 2023; Tomassetti and Di Nicola, 2021). The ideal gas specific heat capacity at constant volume (c^0_{v}) considered in the calculation of c was determined from the gaseous speed of sound in the temperature range from (203 to 383) K measured by Demirdesen et al. (2023). The values of c^0_{v} are reported in Table 5 and were obtained by considering the procedure described in previous studies (Kano et al., 2013; Sun et al., 1997). The following equation of c^0_{v} as a function of the temperature was used in the calculation:

$$c^0_{\mathrm{v}} = -0.0842483 + 0.00366159 \cdot T - 2.714 \cdot 10^{-6} \cdot T^2 \quad (3)$$

where T is the temperature in K. The coefficients of Equation (3) were regressed on the values of Table 5, obtaining an average absolute relative deviation (AARD) of 0.26. The general expression used to calculate AARD is as follows:

$$\mathrm{AARD}(X) \Big/ \% = \frac{100}{N} \sum_{i=1}^{N} \left| \frac{X_{\mathrm{exp},i} - X_{\mathrm{calc},i}}{X_{\mathrm{exp},i}} \right| \quad (4)$$

Table 3
Sets of PC-SAFT parameters for R1132a.

	Set A[a]	Set B[b]
M	2.36233	2.32231
σ/Å	3.21963	3.24150
(ε/k)/K	155.116	156.274

[a] Values reported by Outcalt and Rowane (2022)
[b] Values calculated using the Anoune et al. (2021) correlations with the physical properties of Table 1

Table 4
Average absolute relative deviations (AARD) between literature experimental saturated pressures (p_{sat}), saturated liquid and vapor densities ($\rho^{\mathrm{l}}_{\mathrm{sat}}$ and $\rho^{\mathrm{v}}_{\mathrm{sat}}$), density in the subcooled liquid (ρ^{l}), pressures in the superheated vapor regions (p^{v}), and speed of sound (c) and calculations provided by the PC-SAFT EoS.

	AARD/%	
	Set A[a]	Set B[b]
p_{sat}		
Perera et al. (2023)	0.67	0.39
Thu et al. (2023)	0.86	0.37
Tomassetti and Di Nicola (2021)	1.01	0.29
$\rho^{\mathrm{l}}_{\mathrm{sat}}$		
Perera et al. (2023)	16.99	18.45
$\rho^{\mathrm{v}}_{\mathrm{sat}}$		
Perera et al. (2023)	3.11	2.79
ρ^{l}		
Perera et al. (2023)	9.81	12.79
p^{v}		
Perera et al. (2023)	1.34	1.33
Tomassetti and Di Nicola (2021)	0.40	0.39
C		
Demirdesen et al. (2023)	0.59	0.59
Rowane and Perkins (2024)	1.64	1.45

[a] Values reported by Outcalt and Rowane (2022)
[b] Values calculated using the Anoune et al. (2021) correlations with the physical properties of Table 1

Table 5
Values of the ideal gas specific heat capacity at constant volume (c^0_{v}) of R1132a determined from the speed of sound measured by Demirdesen et al. (2023).

T/K	c^0_{v}/kJ•kg^{-1}•K^{-1}
203.52	0.549071
223.42	0.598706
243.37	0.643828
273.32	0.716613
298.29	0.764276
323.27	0.815816
373.23	0.908860
383.22	0.916611

where X_{exp} is the experimentally determined property and X_{calc} is the calculated property. From the results reported in Table 4, it can be noted that Set B generally ensured lower deviations between the calculated and experimental data. For this reason, the PC-SAFT EoS with this set of parameters (Set B of Table 3) has been used for the calculations reported below.

3. Results and discussion

This section presents the *pvTz* properties for the CO2 + R1132a binary system measured using the isochoric apparatus. Moreover, the experimental data are compared with the values provided by EoSs and molecular simulations.

3.1. *pvTz* measurements

The *pvTz* measurements for CO_2 + R1132a binary system were carried out from (228.15 to 303.15) K along ten isochores (0.016846, 0.018521, 0.028775, 0.029922, 0.029931, 0.032358, 0.037241, 0.039089, 0.052176, 0.083492) m^3•kg^{-1} and ten CO_2 mole fractions (0.1429,0.1473, 0.3315, 0.3323, 0.5003, 0.5458, 0.5666, 0.6954, 0.8614, 0.9027). Fig. 2 shows the *T-p* behaviors of the experimental points in the two-phase and superheated vapor regions. The experimental points show a continuous variation from an exponential curve in the two-phase region to a linear variation in the superheated vapor

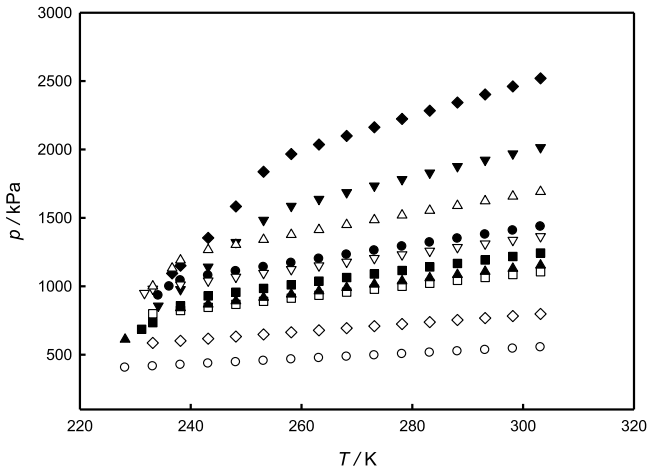


Fig. 2. Measurements of pressure (p), specific volume (v), temperature (T), and bulk mole fraction (z) for the ten isochores of CO_2 (1) + R1132a (2) binary system in the two-phase and superheated vapor regions (Tables 6 and 7); ▲, z_1 = 0.1429 and v = 0.032358 $m^3 \bullet kg^{-1}$; ■, z_1 = 0.1473 and v = 0.029931 $m^3 \bullet kg^{-1}$; ▼, z_1 = 0.3315 and v = 0.018521 $m^3 \bullet kg^{-1}$; ⋄, z_1 = 0.3323 and v = 0.052176 $m^3 \bullet kg^{-1}$; l, z_1 = 0.5003 and v = 0.039089 $m^3 \bullet kg^{-1}$; ●, z_1 = 0.5458 and v = 0.029922 $m^3 \bullet kg^{-1}$; ○, z_1 = 0.5666 and v = 0.083492 $m^3 \bullet kg^{-1}$; ◆, z_1 = 0.6954 and v = 0.016846 $m^3 \bullet kg^{-1}$ Δ, z_1 = 0.8614 and v = 0.028775 $m^3 \bullet kg^{-1}$; ▽, z_1 = 0.9027 and v = 0.037241 $m^3 \bullet kg^{-1}$. Error crosses are not shown since the measurement uncertainties are smaller than the symbols.

region. The two-phase and the vapor-phase experimental data are provided in Tables 6 and 7, respectively.

3.2. Two-phase pvTz calculation and derived VLE properties

The p, x_i, and y_i calculated from the procedure based on the "flash method" with the PR and PC-SAFT EoSs are reported in Table 8. The following average absolute relative deviations of the pressure (AARD (p)) and binary interaction parameters (k_{12}) for the studied EoSs and were obtained: AARD (p) = 0.20 % for the PR EoS with k_{12} = 0.019490 and AARD (p) = 0.19 % for the PC-SAFT EoS with k_{12} = 0.029862. As highlighted in Table 6 (please see the footnote b), different experimental points in the proximity of the superheated vapor region were not

Table 6
Two-phase experimental values of pressure (p), specific volume (v), temperature (T), and bulk mole fraction (z) for the binary system containing CO_2 (1) and R1132a (2)[a].

T/K	p/kPa	v/$m^3 \bullet kg^{-1}$	T/K	p/kPa	v/$m^3 \bullet kg^{-1}$
z_1 = 0.1429			z_1 = 0.5458		
228.15	611.7	0.032302	234.15	933.0	0.029880
238.15[b]	842.4[b]	0.032316[b]	236.15	998.6	0.029882
z_1 = 0.1473			z_1 = 0.6954		
231.15	685.4	0.029886	236.65	1093.8	0.016822
233.15	733.7	0.029888	238.15	1150.8	0.016823
238.15[b]	857.2[b]	0.029895[b]	243.15	1353.9	0.016827
			248.15	1583.3	0.016831
			253.15[b]	1837.2[b]	0.016834[b]
z_1 = 0.3315			z_1 = 0.8614		
234.15	856.6	0.018494	233.15	1000.7	0.028733
238.15	977.0	0.018497	236.65	1131.5	0.028738
243.15	1141.6	0.018501	238.15	1190.7	0.028740
248.15	1321.8	0.018505			
253.15[b]	1483.3[b]	0.018509[b]			
z_1 = 0.5003			z_1 = 0.9027		
228.15	735.9	0.039024	231.65	949.1	0.037185
233.15[b]	799.4[b]	0.039033[b]			

[a] Expanded uncertainties are $U(T)$ = 0.03 K, $U(p)$ = 1 kPa, $U(v)$ = 0.005107 $m^3 \bullet kg^{-1}$, and $U(z_1)$ = 0.0213 at the 95 % confidence level.
[b] Not considered in the regression.

Table 7
Vapor-phase experimental values of pressure (p), specific volume (v), temperature (T), and bulk mole fraction (z) for the binary system containing CO_2 (1) and R1132a (2)[a].

T/K	p/kPa	v/$m^3 \bullet kg^{-1}$	T/K	p/kPa	v/$m^3 \bullet kg^{-1}$
z_1 = 0.1429			z_1 = 0.5458		
243.15[b]	868.7[b]	0.032323[b]	238.15[b]	1042.3[b]	0.029885[b]
248.15	892.9	0.032330	243.15[b]	1078.5[b]	0.029892[b]
253.15	917.8	0.032337	248.15	1109.8	0.029898
258.15	942.1	0.032344	253.15	1140.1	0.029905
263.15	965.3	0.032351	258.15	1170.6	0.029911
268.15	990.2	0.032359	263.15	1200.7	0.029918
273.15	1014.8	0.032366	268.15	1230.8	0.029924
278.15	1038.1	0.032373	273.15	1260.9	0.029931
283.15	1061.5	0.032380	278.15	1290.6	0.029938
288.15	1084.8	0.032387	283.15	1319.7	0.029944
293.15	1107.7	0.032394	288.15	1348.9	0.029951
298.15	1130.4	0.032401	293.15	1378.1	0.029957
303.15	1153.8	0.032408	298.15	1407.3	0.029964
			303.15	1436.0	0.029970
z_1 = 0.1473			z_1 = 0.5666		
243.15[b]	929.2[b]	0.029901[b]	228.15	404.5	0.083355
248.15	956.9	0.029908	233.15	414.7	0.083373
253.15	984.3	0.029915	238.15	425.1	0.083391
258.15	1011.0	0.029921	243.15	435.1	0.083410
263.15	1037.5	0.029928	248.15	445.3	0.083428
268.15	1063.6	0.029934	253.15	455.1	0.083446
273.15	1089.6	0.029941	258.15	465.2	0.083465
278.15	1115.7	0.029947	263.15	475.2	0.083483
283.15	1141.3	0.029954	268.15	485.1	0.083501
288.15	1166.8	0.029961	273.15	495.1	0.083520
293.15	1192.1	0.029967	278.15	505.1	0.083538
298.15	1217.6	0.029974	283.15	514.4	0.083556
303.15	1242.9	0.029980	288.15	524.4	0.083575
			293.15	534.2	0.083593
			298.15	544.2	0.083611
			303.15	553.9	0.083630
z_1 = 0.3315			z_1 = 0.6954		
258.15[b]	1585.7[b]	0.018513[b]	258.15[b]	1967.0[b]	0.016838[b]
263.15	1636.6	0.018517	263.15[b]	2035.9[b]	0.016842[b]
268.15	1685.6	0.018521	268.15	2099.0	0.016845
273.15	1734.0	0.018525	273.15	2162.3	0.016849
278.15	1781.8	0.018529	278.15	2223.4	0.016853
283.15	1829.4	0.018533	283.15	2283.7	0.016857
288.15	1876.4	0.018538	288.15	2342.9	0.016860
293.15	1923.0	0.018542	293.15	2402.4	0.016864
298.15	1968.9	0.018546	298.15	2461.4	0.016868
303.15	2015.0	0.018550	303.15	2519.9	0.016871
z_1 = 0.3323			z_1 = 0.8614		
233.15	585.4	0.052096	243.15[b]	1266.9[b]	0.028746[b]
238.15	601.5	0.052108	248.15[b]	1304.4[b]	0.028752[b]
243.15	617.1	0.052119	253.15	1341.2	0.028759
248.15	632.5	0.052131	258.15	1377.4	0.028765
253.15	648.3	0.052142	263.15	1413.4	0.028771
258.15	663.4	0.052153	268.15	1449.7	0.028778
263.15	677.9	0.052165	273.15	1484.9	0.028784
268.15	693.6	0.052176	278.15	1519.9	0.028790
273.15	708.6	0.052188	283.15	1554.5	0.028796
278.15	723.8	0.052199	288.15	1589.5	0.028803
283.15	738.2	0.052211	293.15	1624.0	0.028809
288.15	753.2	0.052222	298.15	1658.1	0.028815
293.15	767.2	0.052234	303.15	1691.5	0.028822
298.15	782.5	0.052245			
303.15	797.6	0.052257			
z_1 = 0.5003			z_1 = 0.9027		
238.15[b]	822.8[b]	0.039042[b]	233.15[b]	980.2[b]	0.037187[b]
243.15	845.8	0.039050	238.15	1011.6	0.037195
248.15	868.2	0.039059	243.15	1040.0	0.037204
253.15	890.5	0.039067	248.15	1068.1	0.037212
258.15	913.0	0.039076	253.15	1095.8	0.037220
263.15	934.8	0.039085	258.15	1123.2	0.037228
268.15	957.0	0.039093	263.15	1150.5	0.037236
273.15	978.8	0.039102	268.15	1177.6	0.037244
278.15	1000.3	0.039110	273.15	1204.7	0.037253
283.15	1022.0	0.039119	278.15	1231.5	0.037261
288.15	1043.4	0.039127	283.15	1258.0	0.037269
293.15	1064.8	0.039136	288.15	1284.6	0.037277

(continued on next page)

Table 7 (*continued*)

T/K	p/kPa	v/m^3•kg^{-1}	T/K	p/kPa	v/m^3•kg^{-1}
298.15	1086.1	0.039145	293.15	1311.1	0.037285
303.15	1106.7	0.039153	298.15	1337.5	0.037294
			303.15	1363.9	0.037302

[a] Expanded uncertainties are $U(T) = 0.03$ K, $U(p) = 1$ kPa, $U(v) = 0.005107$ m^3•kg^{-1}, and $U(z_1) = 0.0213$ at the 95 % confidence level.
[b] Not considered in the regression.

Table 8
VLE properties calculated from the two-phase measurements of CO_2 (1) + R1132a (2) binary system (Table 6) through the "flash method" with the selected models.

	PR EoS			PC-SAFT EoS		
T/K	p_{calc}/kPa	x_1	y_1	p_{calc}/kPa	x_1	y_1
$z_1 = 0.1429$						
228.15	613.8	0.0981	0.1604	614.2	0.0989	0.1601
$z_1 = 0.1473$						
231.15	685.1	0.1012	0.1635	685.6	0.1019	0.1634
233.15	733.8	0.0993	0.1598	734.2	0.1000	0.1597
$z_1 = 0.3315$						
234.15	855.8	0.2762	0.3808	854.9	0.2774	0.3804
238.15	976.1	0.2700	0.3715	975.0	0.2712	0.3713
243.15	1142.9	0.2618	0.3592	1141.4	0.2631	0.3592
248.15	1328.8	0.2533	0.3460	1326.8	0.2546	0.3463
$z_1 = 0.5003$						
228.15	737.9	0.4016	0.5077	736.8	0.4030	0.5078
$z_1 = 0.5458$						
234.15	936.1	0.4596	0.5570	934.5	0.4607	0.5571
236.15	1000.0	0.4534	0.5509	998.2	0.4545	0.5511
$z_1 = 0.6954$						
236.65	1091.8	0.6657	0.7211	1090.3	0.6653	0.7218
238.15	1148.5	0.6638	0.7198	1146.7	0.6634	0.7204
243.15	1353.0	0.6566	0.7144	1350.3	0.6564	0.7148
248.15	1582.3	0.6482	0.7075	1578.3	0.6482	0.7078
$z_1 = 0.8614$						
233.15	997.1	0.8532	0.8635	999.1	0.8505	0.8642
236.65	1128.4	0.8504	0.8626	1129.9	0.8476	0.8629
238.15	1188.5	0.8491	0.8621	1189.7	0.8463	0.8622
$z_1 = 0.9027$						
231.65	946.7	0.9007	0.9028	950.3	0.8975	0.9029

considered in the calculation since they gave unrealistic high deviations.

Fig. 3 shows the relative deviations between measured pressures and calculated values. Table 8 and Fig. 3 indicate that both models ensured accurate results, providing pressure deviations below 1 % for all the data points. Moreover, as shown in Fig. 3, the results of the two EoSs are in excellent agreement. In particular, the results of the PC-SAFT method using the selected R1132a parameters (Set B of Table 3 and k_{12} = 0.029862) seem to successfully represent the two-phase pressure for the CO_2+R1132a mixture system.

Since no VLE measurements were found in the literature, Fig. 4 shows a comparison between the VLE properties obtained from the MD simulations and the data calculated from the PR EoS with k_{12} = 0.019490 and the PC-SAFT EoS with k_{12} = 0.029862 at 223.15 K, 238.15 K, and 263.15 K. Fig. 4 also presents the experimental p_{sat} for R1132a taken from Tomassetti and Di Nicola (2021) and the p_{sat} calculations for CO_2 provided by REFPROP 10.0 (Lemmon et al., 2018). The results of the MD simulations are reported in Table 9.

Fig. 4 shows that, although the simulated VLE data were not used in the EoS parameter regression, the behaviors provided by the selected models are in qualitative agreement with the simulation results. In particular, the following deviations between the simulated and calculated VLE properties were obtained: the MD simulations deviated from the PR EoS with an AARD an AARD(p_{sim}) of 3.44 % and an average absolute deviation of the vapor mole fraction (AAD(y_{sim})) of 0.0284, while from the PC-SAFT EoS with an AARD(p_{sim}) of 3.32 % and AAD (y_{sim}) of 0.0283. The expressions of AARD(p_{sim}) and AAD(y_{sim}) are as

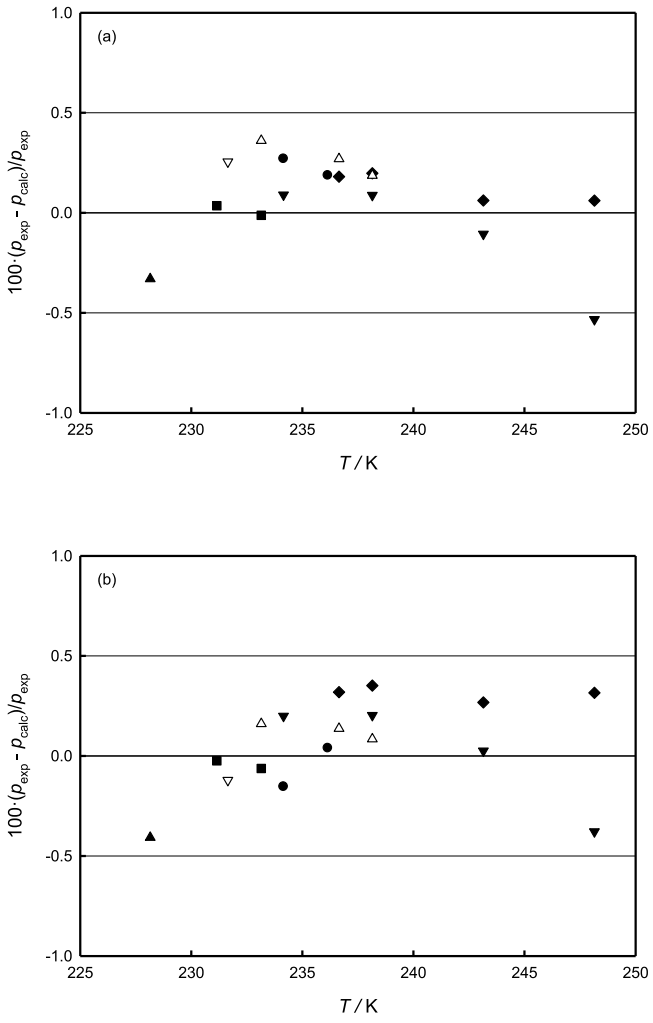


Fig. 3. Relative deviations between the measured two-phase pressures (p_{exp}) of CO_2 (1) + R1132a (2) binary systems (Table 6) and the calculated values (p_{calc}) from the Peng-Robinson EoS (a) and PC-SAFT EoS (b). Symbols indicate different isochores and are defined in Fig. 2.

follows:

$$\mathrm{AARD}(p_{sim})/\% = \frac{100}{N}\sum_{i=1}^{N}\left|\frac{p_{sim,i} - p_{calc,i}}{p_{sim,i}}\right| \quad (5)$$

$$\mathrm{AARD}(y) = \sum_{i=1}^{N}\frac{\left|y_{sim,i} - y_{calc,i}\right|}{N} \quad (6)$$

where p_{sim} and y_{sim} are the simulated pressure and mole fraction of the vapor phase, respectively.

In addition, the selected models are generally in good agreement with the p_{sat} of the pure components, while the MD simulations are in qualitative agreement. Nevertheless, MD simulations can still be considered a valid tool for obtaining qualitative behavior of the thermodynamic properties of mixtures for which experimental data are not available in the open literature.

Finally, the simulation results and model calculations show that the studied binary system exhibits a relatively weak positive deviation from ideality over the temperature and pressure ranges investigated, resulting in azeotropic compositions close to pure CO_2. Azeotropic or near-azeotropic properties are often desirable in system design because they reduce performance degradation of the refrigeration cycle.

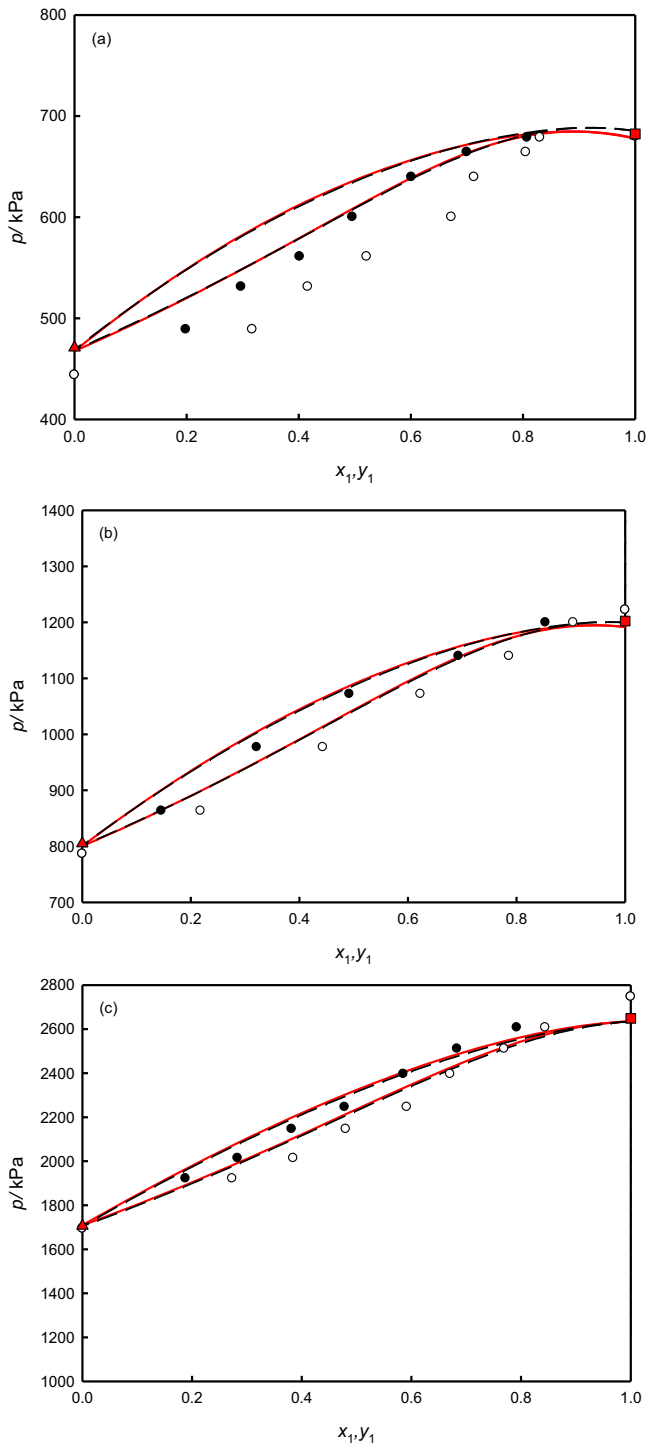


Fig. 4. MD simulation results (circles) and calculated behaviors of the VLE for CO_2 (1) + R1132a (2) binary system through the Peng-Robinson EoS with k_{12} = 0.019490 (red lines) and the PC-SAFT EoS with k_{12} = 0.029862 (dashed lines) at 223.15 K (a), 238.15 K (b), and 263.15 K (c). Red triangles are the experimental p_{sat} for R1132a taken from Tomassetti and Di Nicola (2021). Red squares are the p_{sat} calculations for CO_2 provided by REFPROP 10.0 (Lemmon et al., 2018).

3.3. Vapor-phase *pvTz* calculation

The *pvTz* properties of the CO_2 + R1132a binary system measured in the superheated vapor region were compared with the data provided by the PR and PC-SAFT EoSs. The model calculations were carried out using

Table 9
VLE properties of CO_2 (1) + R1132a (2) binary system (Table 6) obtained from MD simulations.

p_{calc}/kPa	x_1	y_1	z_1 [a]
T = 223.15 K			
444.0	0.000	0.000	-
489.0	0.199	0.317	0.2000
531.2	0.297	0.416	0.3000
561.1	0.402	0.521	0.4000
600.2	0.496	0.672	0.5000
639.7	0.601	0.713	0.6000
664.4	0.700	0.805	0.7000
678.9	0.807	0.830	0.8000
680.0	1.000	1.000	-
T = 238.15 K			
786.7	0.000	0.000	-
863.5	0.146	0.218	0.1473
977.0	0.321	0.443	0.3313
1072.1	0.492	0.623	0.5000
1139.9	0.693	0.786	0.6953
1200.0	0.853	0.904	0.8613
1222.4	1.000	1.000	-
T = 263.15 K			
1694.4	0.000	0.000	-
1921.9	0.188	0.273	0.8000
2014.2	0.283	0.385	0.7000
2146.6	0.382	0.480	0.6000
2246.3	0.478	0.592	0.5000
2396.3	0.585	0.671	0.7000
2511.0	0.683	0.769	0.3000
2607.9	0.792	0.844	0.2000
2747.3	1.000	1.000	-

[a] Packed mole fraction

k_{12} obtained from the procedure based on the "flash method". As highlighted in Table 7 (see the footnote b), different measurements in the proximity of the two-phase region were not considered in the calculation since they gave unrealistic high deviations.

Fig. 5 shows the deviations between the experimental pressures of the CO_2 + R1132a binary system and the values provided by the selected EoSs. It is evident that consistent and accurate results were given by both models, yielding deviations always lower than ±1 % for all the points. This outcome is also confirmed by the obtained AARD(p) which are equal to 0.38 % for PR EoS with k_{12} = 0.01949 and 0.33 % for PC-SAFT EoS with k_{12} = 0.029862. The PC-SAFT method is the most representative of the experimental values with the smallest deviation.

The vapor-phase *pvTz* property of the measured binary system derived from molecular simulations are reported in Table 10 and Fig. 6. A qualitative agreement between the simulated data and the *pvTz* measurements is evident in Fig. 6. This outcome is confirmed by the low deviations between the simulated values and the calculations provided by the EoSs: AARD(p) = 1.02 % for the PR EoS and AARD(p) = 1.00 % for the PC-SAFT EoS. The calculated results above 303.15 K are in the extrapolated range without experimental values used in the regression method. However, as evident in Fig. 6, the calculated values and MD are in qualitatively good agreement.

Finally, the 49 vapor densities measured by Menegazzo et al. (2025) for two compositions of the CO_2 (1) + R1132a (2) binary system (z_1 = 0.5942 and 0.7926) were compared with the calculations provided by the PR EoS with k_{12} = 0.01949 and the PC-SAFT EoS with k_{12} = 0.029862. Both models provided AARD(p) of 0.27 %, confirming the reliability of the presented measurements and models.

4. Conclusions

In this study, 23 two-phase and 133 vapor-phase *pvTz* properties for the CO_2 + R1132a binary system measured by using an isochoric apparatus were presented. In addition, although the accuracy is lower than that of the experiments, molecular dynamics (MD) simulations were conducted to extrapolate the VLE and vapor-phase *pvTz* properties

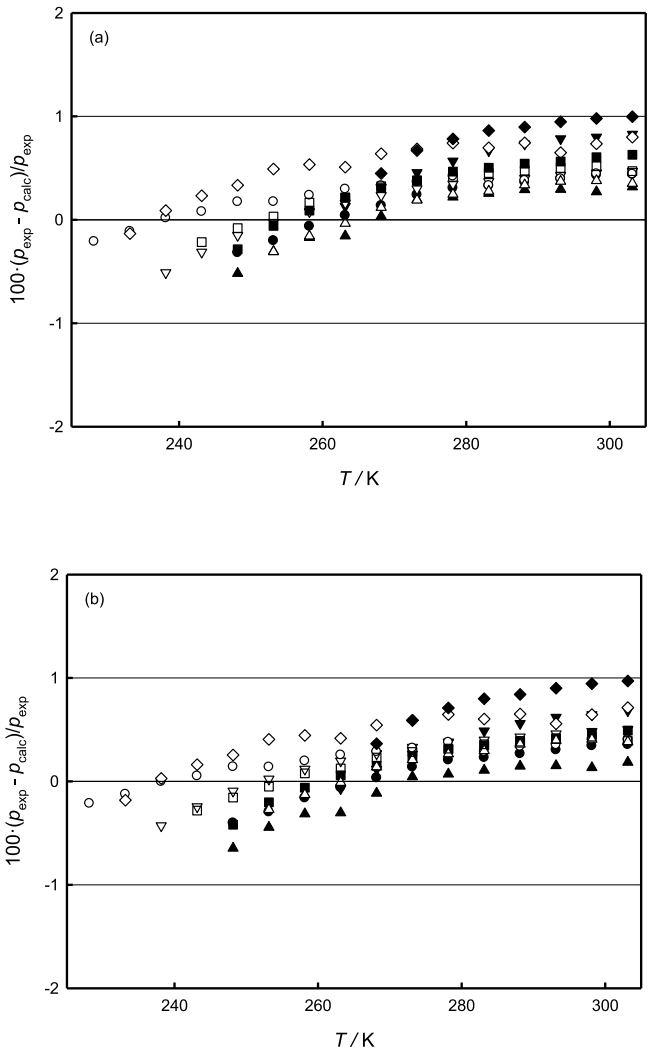


Fig. 5. Deviations between the vapor-phase pressures (p_{exp}) of CO_2 (1) + R1132a (2) binary system (Table 7) and the pressures (p_{calc}) provided by the PR EoS with k_{12} = 0.023561 (a) and PC-SAFT EoS with k_{12} = 0.031251 (c). Symbols indicate different isochores and are defined in Fig. 2.

Table 10
Vapor-phase MD simulated values of pressure (p), specific volume (v), temperature (T), and bulk mole fraction (z) for the binary system containing CO_2 and R1132a.

T/K	p/kPa	v/m^3•kg^{-1}
z_1 = 0.1429		
243.15	874.2	0.032366
263.15	975.1	0.032366
283.15	1072.7	0.032366
303.15	1162.8	0.032366
363.15	1441.5	0.032366
443.15	1799.9	0.032366
z_1 = 0.3323		
253.15	635.3	0.052176
273.15	694.0	0.052176
303.15	788.2	0.052176
363.15	951.5	0.052176
443.15	1198.4	0.052176
z_1 = 0.5458		
303.15	1451.1	0.029928
443.15	2264.4	0.029928

of the studied mixture.

The main results of the present work are as follows:

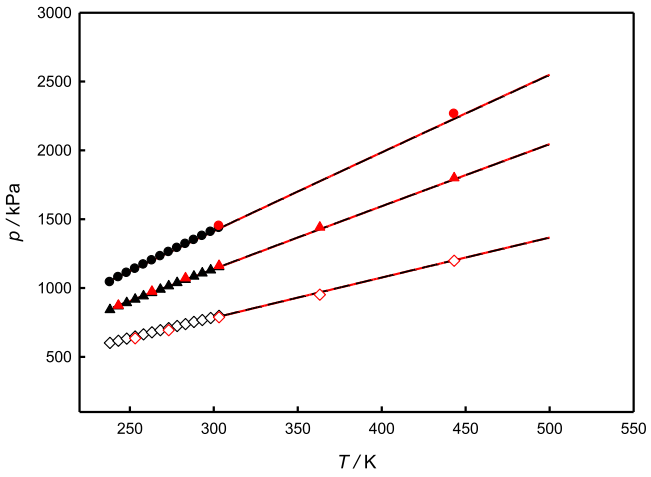


Fig. 6. *pvTz* measurements (black) and MD simulations (red) for three isochores of CO_2 (1) + R1132a (2) binary system in the superheated vapor region (Table 7) showing how MD simulations can be used to extend the data to higher temperatures; ▲, z_1 = 0.1429 and v = 0.032358 m^3•kg^{-1}; ▲, z_1 = 0.1429 and v = 0.032366 m^3•kg^{-1}; ◇, z_1 = 0.3323 and v = 0.052176 m^3•kg^{-1}; ◇, z_1 = 0.3323 and v = 0.052176 m^3•kg^{-1}; ●, z_1 = 0.5458 and v = 0.029922 m^3•kg^{-1}; ●, z_1 = 0.5458 and v = 0.029928 m^3•kg^{-1}. The red and dashed lines are the behaviors calculated through the PR and PC-SAFT EoSs, respectively. Error crosses are not shown since the measurement uncertainties are smaller than the symbols.

- The measurements in the two-phase region were employed to derive the VLE properties by using the flash method with the PR and PC-SAFT equations of state (EoSs). The two models ensured similar results and low deviations for the pressures (AARD (p) = 0.20 % for the PR EoS and AARD (p) = 0.19 % for the PC-SAFT EoS). A qualitatively good agreement between the VLE assessed with the flash method and the results provided by the MD simulations was also found.
- The vapor-phase measurements showed also a qualitatively good agreement with the values predicted through the MD simulations. In addition, the vapor-phase experimental and simulated *pvTz* properties were compared with the values provided by the PR and PC-SAFT EoSs. Both models provided an accurate description of the measurements, obtaining AARD(p) equal to 0.38 % for PR EoS and 0.33 % for PC-SAFT EoS. The MD simulations in the superheated vapor region showed a qualitatively good agreement with the calculations provided by the EoSs (AARD(p) = 1.02 % for the PR EoS and AARD (p) = 1.00 % for the PC-SAFT EoS). Although MD calculations exhibit significant errors and cannot currently replace measurements, they are useful for verifying extrapolated regions and screening mixtures where no measurement data exists.
- The measurement data, together with the MD simulations and EoS correlations provided in this study, can serve as a basis for evaluating candidate refrigerants for ultra-low-temperature applications. In particular, the presented data could be used to develop accurate thermodynamic models for evaluating the performance of mixtures containing the studied refrigerants in ULT systems.

CRediT authorship contribution statement

Sebastiano Tomassetti: Writing – review & editing, Writing – original draft, Visualization, Validation, Investigation, Conceptualization. **Lorenzo Merlonghi:** Writing – review & editing, Validation, Software. **Tomoaki Imai:** Software, Methodology. **Giovanni Di Nicola:** Writing – review & editing, Supervision. **Chieko Kondou:** Writing – review & editing, Writing – original draft, Software, Methodology, Data curation.

Declaration of competing interest

The authors declare that they have no known competing financial interests or personal relationships that could have appeared to influence the work reported in this paper.

Acknowledgements

This molecular dynamics simulation study was funded by Japan Science and Technology agency “Fusion Oriented Research for disruptive Science and Technology (FOREST)”, no. JPMJFR2172.

Supplementary materials

Supplementary material associated with this article can be found, in the online version, at doi:10.1016/j.ijrefrig.2026.01.002.

References

Abraham, M.J., Murtola, T., Schulz, R., Páll, S., Smith, J.C., Hess, B., Lindah, E., 2015. Gromacs: High performance molecular simulations through multi-level parallelism from laptops to supercomputers. SoftwareX. 1–2, 19–25. https://doi.org/10.1016/j.softx.2015.06.001.

Anoune, I., Mimoune, Z., Madani, H., Merzougui, A., 2021. New modified PC-SAFT pure component parameters for accurate VLE and critical phenomena description. Fluid. Phase Equilib. 532, 112916. https://doi.org/10.1016/j.fluid.2020.112916.

ASHRAE Standard, 2022. Designation and safety classification of refrigerants. ANSI/ASHRAE Stand. 34.

Bai, T., Li, D., Xie, H., Yan, G., Yu, J., 2021. Experimental research on a Joule-Thomson refrigeration cycle with mixture R170/R290 for- 60°C low-temperature freezer. Appl. Therm. Eng. 186, 116476. https://doi.org/10.1016/j.applthermaleng.2020.116476.

Bell, I.H., 2025. Modeling Mixtures Containing Refrigerants: Updated Interaction Parameters. J. Chem. Eng. Data 70, 1173–1181. https://doi.org/10.1021/acs.jced.4c00699.

Bell, I.H., Deiters, U.K., Leal, A.M.M., 2022. Implementing an equation of state without Derivatives: teqp. Ind. Eng. Chem. Res. 61, 6010–6027. https://doi.org/10.1021/acs.iecr.2c00237.

Bell, I.H., Riccardi, D., Bazyleva, A., McLinden, M.O., 2021. Survey of Data and Models for Refrigerant Mixtures Containing Halogenated Olefins. J. Chem. Eng. Data 66 (6), 2335–2354. https://doi.org/10.1021/acs.jced.1c00192.

Bell, I.H., Welliquet, J., Mondejar, M.E., Bazyleva, A., Quoilin, S., Haglind, F., 2019. Application of the group contribution volume translated Peng–Robinson equation of state to new commercial refrigerant mixtures. Int. J. Refrig. 103, 316–328. https://doi.org/10.1016/j.ijrefrig.2019.04.014.

Berendsen, H.J.C., van der Spoel, D., van Drunen, R., 1995. GROMACS: A message-passing parallel molecular dynamics implementation. Comput. Phys. Commun. 91, 43–56. https://doi.org/10.1016/0010-4655(95)00042-E.

Brown, J.S., Coccia, G., Tomassetti, S., Pierantozzi, M., Di Nicola, G., 2018. Vapor Phase PvTx Measurements of Binary Blends of trans-1-Chloro-3,3,3-trifluoroprop-1-ene + Isobutane and cis-1,3,3,3-Tetrafluoroprop-1-ene + Isobutane. J. Chem. Eng. Data 63, 169–177. https://doi.org/10.1021/acs.jced.7b00769.

Brown, J.S., Coccia, G., Tomassetti, S., Pierantozzi, M., Di Nicola, G., 2017. Vapor Phase PvTx Measurements of Binary Blends of 2,3,3,3-Tetrafluoroprop-1-ene + Isobutane and trans-1,3,3,3-Tetrafluoroprop-1-ene + Isobutane. J. Chem. Eng. Data 62, 3577–3584. https://doi.org/10.1021/acs.jced.7b00564.

Cuendet, M.A., Van Gunsteren, W.F., 2007. On the calculation of velocity-dependent properties in molecular dynamics simulations using the leapfrog integration algorithm. J. Chem. Phys. 127. https://doi.org/10.1063/1.2779878.

Darden, T., York, D., Pedersen, L., 1993. Particle mesh Ewald: An N·log(N) method for Ewald sums in large systems. J. Chem. Phys. 98, 10089–10092. https://doi.org/10.1063/1.464397.

Delhommelle, J., Millié, P., 2001. Inadequacy of the Lorentz-Berthelot combining rules for accurate predictions of equilibrium properties by molecular simulation. Mol. Phys. 99, 619–625. https://doi.org/10.1080/00268970010020041.

Demirdesen, D., Wedler, C., Low, R.E., Trusler, J.P.M., 2023. Speed of Sound in Gaseous 1, 1-Difluoroethene (R1132a) at Temperatures Between 193 K and 383 K at Pressures up to 3 MPa. Int. J. Thermophys. 44, 90. https://doi.org/10.1007/s10765-023-03198-y.

Di Nicola, G., Giuliani, G., Passerini, G., Polonara, F., Stryjek, R., 1998. Vapor-Liquid-Equilibrium (VLE) properties of R-32 + R-134a system derived from isochoric measurements. Fluid. Phase Equilib. 153, 143–165. https://doi.org/10.1016/S0378-3812(98)00407-5.

Di Nicola, G., Polonara, F., Ricci, R., Stryjek, R., 2005. PVTx measurements for the R116 + CO_2 and R41+ CO_2 systems. New isochoric apparatus. J. Chem. Eng. Data 50, 312–318. https://doi.org/10.1021/je049939g.

Di Nicola, G., Polonara, F., Stryjek, R., Arteconi, A., 2011. Performance of cascade cycles working with blends of CO2+ natural refrigerants. Int. J. Refrig. 34, 1436–1445. https://doi.org/10.1016/j.ijrefrig.2011.05.004.

Domanski, P.A., McLinden, M.O., 2025. Updating the limited options for low-global-warming-potential refrigerants. Int. J. Refrig. 178, 410–417. https://doi.org/10.1016/j.ijrefrig.2025.07.011.

Fouad, W.A., Alasiri, H., 2020. Molecular dynamic simulation and SAFT modeling of the viscosity and self-diffusion coefficient of low global warming potential refrigerants. J. Mol. Liq. 317, 113998. https://doi.org/10.1016/j.molliq.2020.113998.

Fouad, W.A., Vega, L.F., 2018. Next generation of low global warming potential refrigerants: Thermodynamic properties molecular modeling. AIChe J. 64, 250–262. https://doi.org/10.1002/aic.15859.

Giménez-Prades, P., Udroiu, C.M., Navarro-Esbrí, J., Mota-Babiloni, A., 2025. Thermodynamic Evaluation of Low-GWP A1 Refrigerants for Ultra-Low Temperature Refrigeration Applications. Energies. (Basel) 18, 4428. https://doi.org/10.3390/en18164428.

Giuliani, G., Kumar, S., Polonara, F., 1995. A constant volume apparatus for vapour pressure and gas phase P-ν-T measurements: validation with data for R22 and R134a. Fluid. Phase Equilib. 109, 265–279. https://doi.org/10.1016/0378-3812(95)02727-V.

Gross, J., Sadowski, G., 2001. Perturbed-chain SAFT: An equation of state based on a perturbation theory for chain molecules. Ind. Eng. Chem. Res. 40, 1244–1260. https://doi.org/10.1021/ie0003887.

Hao, Z., He, G., Tian, Q., Cai, D., 2024. Vapor-liquid equilibrium data and performance analysis on binary mixture of R32 and R1216 for residential air condition system. Int. J. Refrig. 157, 127–136. https://doi.org/10.1016/j.ijrefrig.2023.11.009.

Hao, Z., Wu, A., Zhang, Z., Hua, J., Lin, Y., Cai, D., 2025. Comprehensive assessment of high-temperature heat pumps using novel low-GWP refrigerant mixtures as working fluids: Energy, exergy, thermal properties, and safety. Therm. Sci. Eng. Prog. 64, 103786. https://doi.org/10.1016/j.tsep.2025.103786.

Harris, J.G., Yung, K.H., 1995. Carbon dioxide’s liquid-vapor coexistence curve and critical properties as predicted by a simple molecular model. J. Phys. Chem. 99, 12021–12024. https://doi.org/10.1021/j100031a034.

Hess, B., Bekker, H., Berendsen, H.J.C., Fraaije, J.G.E.M., 1997. LINCS: A Linear Constraint Solver for molecular simulations. J. Comput. Chem. 18, 1463–1472. https://doi.org/10.1002/(SICI)1096-987X(199709)18:12<1463::AID-JCC4>3.0.CO;2-H.

Hoover, W.G., 1985. Canonical dynamics: Equilibrium phase-space distributions. Phys. Rev. a 31, 1695. https://doi.org/10.1103/PhysRevA.31.1695.

Imai, T., Miura, T., Hashimoto, M., Okumura, T., Kondou, C., 2023. Molecular simulation for property prediction of low GWP refrigerant mixtures. 26th International Congress of Refrigeration, Paris, FR. https://doi.org/10.18462/iir.10.18462/iir.icr.2023.0877.

Jorgensen, W.L., Maxwell, D.S., Tirado-Rives, J., 1996. Development and testing of the OPLS all-atom force field on conformational energetics and properties of organic liquids. J. Am. Chem. Soc. 118, 11225–11236. https://doi.org/10.1021/ja9621760.

Kano, Y., Kayukawa, Y., Fujii, K., Sato, H., 2013. Ideal gas heat capacity derived from speed of sound measurements in the gaseous phase for trans -1,3,3,3-tetrafluoropropene. J. Chem. Eng. Data 58, 2966–2969. https://doi.org/10.1021/je4004564.

Kawahara, T., Imai, T., Okumura, T., Kondou, C., 2023. Molecular simulation and experimental validation for surface tension of new Low-GWP refrigerant mixtures R32/CF3I and R1123/CF3I. J. Mol. Liq. 386, 122532. https://doi.org/10.1016/j.molliq.2023.122532.

Lemmon, E.W., Bell, I.H., Huber, M.L., McLinden, M.O., 2018. NIST Standard Reference Database 23: Reference Fluid Thermodynamic and Transport Properties-REFPROP, Version 10.0, 2018. National Institute of Standards and Technology. URL. https://www.nist.gov/srd/nist23.cfm.

Low, R., 2018. Evaluation of potential use of R-1132a as a Refrigerant blend component, in: Proceedings of the 1st IIR International Conference on the Application of HFO Refrigerants. Birmingham, UK, p. 13. https://doi.org/10.18462/iir.hfo.2018.1183.

Massuchetto, L.H.P., do Nascimento, R.B.C., de Carvalho, S.M.R., de Araújo, H.V., d’Angelo, J.V.H., 2019. Thermodynamic performance evaluation of a cascade refrigeration system with mixed refrigerants: R744/R1270, R744/R717 and R744/RE170. Int. J. Refrig. 106, 201–212. https://doi.org/10.1016/j.ijrefrig.2019.07.005.

McLinden, M.O., Huber, M.L., 2020. (R) Evolution of refrigerants. J. Chem. Eng. Data 65, 4176–4193. https://doi.org/10.1021/acs.jced.0c00338.

Menegazzo, D., Rowane, A.J., Lombardo, G., Bobbo, S., Fedele, L., McLinden, M.O., 2025. Compressed liquid density and speed of sound measurements and correlation of the binary mixture {carbon dioxide (CO2) + 1,1-difluoroethene (R1132a)} at temperatures from 220 K to 350 K. Int. J. Refrig. 172, 1–16. https://doi.org/10.1016/j.ijrefrig.2025.01.014.

METI, 2019. Act on Rational Use and Proper Management of Fluorocarbons (Fluorocarbon Emissions Control Act). https://www.env.go.jp/earth/furon/files/englishmaterial_rev.pdf (accessed 5th April 2022).

Mota-Babiloni, A., Fernández-Moreno, A., Giménez-Prades, P., Udroiu, C.-M., Navarro-Esbrì, J., 2023. Ternary refrigerant blends for ultra-low temperature refrigeration. Int. J. Refrig. 148, 108–116. https://doi.org/10.1016/j.ijrefrig.2023.01.006.

Mota-Babiloni, A., Joybari, M.M., Navarro-Esbrì, J., Mateu-Royo, C., Barragán-Cervera, Á., Amat-Albuixech, M., Molés, F., 2020. Ultralow-temperature refrigeration systems: Configurations and refrigerants to reduce the environmental impact. Int. J. Refrig. 111, 147–158. https://doi.org/10.1016/j.ijrefrig.2019.11.016.

Mota-Babiloni, A., Navarro-Esbrí, J., Molés, F., Cervera, Á.B., Peris, B., Verdú, G., 2016. A review of refrigerant R1234ze(E) recent investigations. Appl. Therm. Eng. 95, 211–222. https://doi.org/10.1016/j.applthermaleng.2015.09.055.

Nosé, S., 1984. A unified formulation of the constant temperature molecular dynamics methods. J. Chem. Phys. 81, 511–519. https://doi.org/10.1063/1.447334.

Outcalt, S.L., Rowane, A.J., 2022. Bubble Point Measurements of Three Binary Mixtures of Refrigerants: R-32/1234yf, R-32/1234ze (E), and R-1132a/1234yf. J. Chem. Eng. Data 67, 932–940. https://doi.org/10.1021/acs.jced.1c00871.

Peng, D.-Y., Robinson, D.B., 1976. A New Two-Constant Equation of State. Ind. Eng. Chem. Fundam. Eng. Chem. Fundam. 15, 11–18. https://doi.org/10.1073/pnas.15.1.11.

Peng, S., Wang, E., Qing, K., Yang, Z., Duan, Y., 2024. Prediction of vapor-liquid equilibrium and pvTx properties of mixtures containing HFOs, HFCs, HCs, and CO2 using polar PC-SAFT model. Fluid. Phase Equilib. 580, 114049. https://doi.org/10.1016/j.fluid.2024.114049.

Perera, U., Miyane, K., Sakoda, N., Thu, K., Higashi, Y., 2023. PvT Properties and Thermodynamic Property Correlations for the Low Global Warming Potential Hydrofluoroolefin Refrigerant R-1132a (1, 1-Difluoroethene). Int. J. Thermophys. 44, 84. https://doi.org/10.1007/s10765-023-03184-4.

Polonara, F., Kuijpers, L., Peixoto, R., 2017. Potential impacts of the Montreal Protocol Kigali Amendment to the choice of refrigerant alternatives. Int. J. Heat Technol. 35, S1–S8. https://doi.org/10.18280/ijht.35Sp0101.

Qin, Y., Li, N., Zhang, H., Liu, B., 2023. A thermodynamic analysis of the Linde-Hampson cycle using low-GWP R1234yf-blends. Case Stud. Therm. Eng. 49, 103358. https://doi.org/10.1016/j.csite.2023.103358.

Qin, Y., Li, N., Zhang, H., Liu, B., 2021a. Energy and exergy analysis of a Linde-Hampson refrigeration system using R170, R41 and R1132a as low-GWP refrigerant blend components to replace R23. Energy 229, 120645. https://doi.org/10.1016/j.energy.2021.120645.

Qin, Y., Li, N., Zhang, H., Liu, B., 2021b. Energy and exergy performance evaluation of a three-stage auto-cascade refrigeration system using low-GWP alternative refrigerants. Int. J. Refrig. 126, 66–75. https://doi.org/10.1016/j.ijrefrig.2021.01.028.

Raabe, G., 2019. Molecular simulation studies on refrigerants past – present – future. Fluid. Phase Equilib. 485, 190–198. https://doi.org/10.1016/j.fluid.2018.12.022.

Raabe, G., 2016. Molecular simulation studies in hydrofluoroolefine (HFO) working fluids and their blends. Sci. Technol. Built. Environ. 22, 1077–1089. https://doi.org/10.1080/23744731.2016.1206796.

Raabe, G., 2015. Molecular Simulation Studies on the Vapor-Liquid Equilibria of the cis- and trans-HCFO-1233zd and the cis-and trans-HFO-1336mzz. J. Chem. Eng. Data 60, 2412–2419. https://doi.org/10.1021/acs.jced.5b00286.

Raabe, G., 2013. Molecular simulation studies on the vapor-liquid phase equilibria of binary mixtures of R-1234yf and R-1234ze(E) with R-32 and CO2. J. Chem. Eng. Data. https://doi.org/10.1021/je4002619.

Regulation (EU) No. 2024/573, 2024. Regulation (EU) No 2024/573 of the European Parliament and of the Council of 7 February 2024 on fluorinated greenhouse gases, amending Directive (EU) 2019/1937 and repealing Regulation (EU) No 517/2014.

Rowane, A.J., Perkins, R.A., 2024. Speed of Sound Measurements of Binary Mixtures of 1,1-Difluoroethylene (R-1132a) + Propane and Derived Speed of Sound of Pure R-1132a. Int. J. Thermophys. 45, 148. https://doi.org/10.1007/s10765-024-03431-2.

Sobieraj, M., Rosiński, M., 2019. High phase-separation efficiency auto-cascade system working with a blend of carbon dioxide for low-temperature isothermal refrigeration. Appl. Therm. Eng. 161, 114149. https://doi.org/10.1016/j.applthermaleng.2019.114149.

Span, R., Wagner, W., 1996. A New Equation of State for Carbon Dioxide Covering the Fluid Region from the Triple-Point Temperature to 1100 K at Pressures up to 800 MPa. J. Phys. Chem. Ref. Data 25, 1509–1596. https://doi.org/10.1063/1.555991.

Sun, L.-Q., Duan, Y.-Y., Shi, L., Zhu, M.-S., Han, L.-Z., 1997. Speed of sound and ideal-gas heat capacity at constant pressure of gaseous difluoromethane. J. Chem. Eng. Data 42, 795–799. https://doi.org/10.1021/je970035n.

Thu, K., Perera, U.A., Miyane, K., Sakoda, N., Higashi, Y., 2023. Vapour Pressure Measurements and Correlations for 1, 1-Difluoroethene (R-1132a) at 240–296 K using a Newly Developed Isochoric Apparatus. Int. J. Thermophys. 44, 61. https://doi.org/10.1007/s10765-023-03167-5.

Tomassetti, S., Coccia, G., Pierantozzi, M., Di Nicola, G., Brown, J.S., 2020a. Vapor Phase and Two-Phase PvTz Measurements of Difluoromethane+ 2, 3, 3, 3-Tetrafluoroprop-1-ene. J. Chem. Thermodyn., 105966 https://doi.org/10.1016/j.jct.2019.105966.

Tomassetti, S., Di Nicola, G., 2021. Saturated pressure and vapor-phase pvT measurements of 1, 1-difluoroethene (R1132a). Fluid. Phase Equilib. 533, 112939. https://doi.org/10.1016/j.fluid.2021.112939.

Tomassetti, S., Di Nicola, G., Kondou, C., 2022a. Triple point measurements for new low-global-warming-potential refrigerants: Hydro-fluoro-olefins, hydro-chloro-fluoro-olefins, and trifluoroiodomethane. Int. J. Refrig. 133, 172–180. https://doi.org/10.1016/j.ijrefrig.2021.10.008.

Tomassetti, S., Di Nicola, G., Miyoshi, K., Busby, S.R., Kondou, C., 2022b. Solid–liquid equilibria of binary systems containing low global warming potential refrigerants. Int. J. Refrig. 144, 254–263. https://doi.org/10.1016/j.ijrefrig.2022.08.016.

Tomassetti, S., Perera, U.A., Di Nicola, G., Pierantozzi, M., Higashi, Y., Thu, K., 2020b. Two-Phase and Vapor-Phase Thermophysical Property (pvTz) Measurements of the Difluoromethane + trans-1,3,3,3-Tetrafluoroprop-1-ene Binary System. J. Chem. Eng. Data 65, 1554–1564. https://doi.org/10.1021/acs.jced.9b00995.

UNEP, 2016. Amendment to the Montreal Protocol on Substances that Deplete the Ozone Layer (Kigali Amendment). Int. Leg. Mater. https://doi.org/10.1017/ilm.2016.2.